RSC Advances

ROYAL SOCIETY OF CHEMISTRY

www.rsc.org/advances

Journal Name

RSCPublishing

ARTICLE

Ionic liquid electrodeposition of Ge nanostructures on freestanding Ni-nanocone arrays for Li-ion battery

Cite this: DOI: 10.1039/xoxxoooooox

Received ooth January 2012,
Accepted ooth January 2012

DOI: 10.1039/xoxxoooooox

www.rsc.org/

Jian Hao‡ [a,b], Xin Liu‡ [a,d], Xusong Liu [a], Xiaoxu Liu[a], Na Li [a], Xiaoxuan Ma [a], Yi Zhang [c], Yao Li [c]*, Jiupeng Zhao [a,b]*

With the growing demand for portable and wearable electronic devices, it is imperative to develop high-performance Li-ion batteries with long lifetimes. The deployment of three-dimensional (3D) nanostructured materials on current collectors has recently emerged as a promising strategy for preparing high-performance Li-ion batteries. We develop a simple and efficient method for fabricating ultrathin and flexible 3D Ge-Ni nanocone arrays (NCAs) electrode materials using a two-step electrodeposition process. With uniform NCAs as the substrate, Ge nanoparticles were deposited from ionic liquid at room temperature. The electrode can be removed from the carrier film. Thus, the resulting freestanding electrode can be as thin as 3 μm and exhibits specific capacity up to 500 mAh/g after 100 cycles at 0.1 C, the rate capability at 1 C and 2 C rates of 700 mAh/g and 400 mAh/g, respectively. This improved electrochemical performance is the result of the 3D NCAs enhanced electron migration and electron transport paths while also providing sufficient elasticity to buffer the volume expansion of the Ge nanoparticles.

Introduction

The development of high-capacity Li-ion battery (LIBs) with long lifetimes has been steadily increasing for use in future power tools, such as portable electronics and electric/hybrid vehicles.[1-3] Materials based on group IVA elements (Si, Ge) have recently attracted attention for LIBs because they offer high specific capacities (Si: 4200 mAh/g[4], Ge: 1600 mAh/g[5]) that are orders of magnitude beyond that of conventional graphite (372 mAh/g). Geranium has received less attention than Si due to its lower capacity. However, the Li diffusion rate is faster in Ge than in Si, which means that Ge may be an attractive electrode material for high charging rate LIBs.[6,7] Furthermore, Ge has been targeted to replace carbon as one of the most promising negative electrodes, which has received extensive research efforts. Unfortunately, a tremendous volume change will inevitably occur during the charge and discharge process, which induces severe pulverization and shedding from the current collector. As a result, capacity fading and poor cycling performance are always observed when using this kind of material.[8] Hence, the realization of a stable energy delivery for commercial applications of alloy anodes in LIBs is still challenging.

To overcome these drawbacks, extensive efforts have been performed to increase capacity retention with battery cycling. One effective strategy is to design specific composites that could provide spaces to buffer the large volume change. For example, Ge/C, [9,10] Ge/Si[11], Ge/multi-walled nanotubes (MWNTs)[12], Ge/Sn[13], and Ge/graphene[14]. Another promising approach is to develop nanostructured morphologies for Ge-based anodes to accommodate volume expansion, such as nanoparticles[15], nanorods[16], nanoline[17], nano-springs[18], nanotubes[19], three-dimensional (3D) porous nanostructures[20], and arrays of nanostructures[21]. These nanoarchitectured electrode configurations enlarged the effective surface area of the electrode; moreover, they are very suitable for relieving mechanical and structural strain during the charge/discharge process. There are a variety of methods for preparing nanostructured Ge-based materials, such as chemical vapor deposition (CVD)[22], electron beam evaporation[23], and magnetron sputtering[24]. Although the electrochemical performance of the composite anodes produced using these methods was attractive, most of the preparation routes are too complicated or require a high reaction temperature, limiting their industrial implementation. Compared with the above recently reported

methods, ionic liquid electrodeposition can be used to achieve semiconductor deposition that cannot be obtained in aqueous solutions at room temperature due to ionic liquids, which have wide electrochemical windows of up to ±3 V compared to the normal hydrogen electrode (NHE), low vapor pressures, and good thermal stability.[25]

Nickel, which is used as the current collector in LIBs, has excellent mechanical properties.[26] Currently, Ni nanocones arrays (NCAs) are used in the comprehensive support of activity materials for the anode in lithium ion batteries. Du and Zhang have synthesized NCAs supporting Sn-Co-based films using electrodeposition[27]. Deyan He et al. have prepared Si-coated NCA anodes using plasma-enhanced chemical vapor deposition.[28] The NCAs facilitated charge collection and transport, supported the electrode structure, and functioned as the inactive confining buffer to accommodate volume variation as well as structural support to enhance the adhesion strength between the active materials and current collectors.

In this study, we have developed a unique Ge nanoarchitecture supported by NCAs composed of nanoscale cylinders as the electrode material for LIBs using ionic liquid electrodeposition. In this configuration, these nanostructured Ge electrodes showed improved cycle stability and rate capability. Moreover, the ionic liquid electrodeposition can be simply controlled using the current value and deposition time to control the thickness of the deposited layer, which can, in turn, prevent high voltage, high temperature, and high vacuum in the Ge preparation procedures reported in other studies.

Experimental

The NCAs were electrodeposited onto Ni foil from a bath consisting of 1-M $NiCl_2 \cdot 6H_2O$, 0.5-M H_3BO_3, and 4.0 M NH_4Cl. The solution was maintained at a temperature of 50–60°C and had a pH of 4.0. The electrodeposition process was performed at a current density of 25 mA/cm^2 for 4 min. The obtained electrodes were successively washed with distilled water and acetone and then dried at 60°C in a vacuum environment.

The ionic liquid 1-ethyl-3-methylimidazolium bis (trifluoromethylsulfonyl) amide, ([Emim]Tf_2N, 99%) was purchased from IOLITEC (Germany) and used after drying under vacuum at 100°C for 24 h. The $GeCl_4$ (99.998%) was purchased from Alfa Aesar. The electrochemical experiments were performed in an argon-filled glove box with water and oxygen contents below 2 ppm (Vigor Glove Box, Suzhou, China). To assemble the three-electrode system, NCAs were used as a working electrode (WE), and a Pt ring and an Ag wire were used as the counter electrode and quasi-reference electrode, respectively. The electrolyte was a 0.1 mol/L $GeCl_4$ and EmimTf_2N solution.

Electrochemical measurements were performed using a VersaStat 2273 (Princeton Applied Research) potentiostat/galvanostat. Cyclic voltammetry (CV) measurements were performed at a scan rate of 10 mV/s across a range of -2.8–0.5 V relative to the quasi reference electrode at 25°C. The electrodeposition time is 30 min. After the experiments, the deposited sediments are rinsed with isopropanol.

The morphology and element distribution of the electrodes were investigated by field emission-scanning electron microscopy (FE-SEM; Hitachi S-4800) operating at 20 kV. Electrochemical charge-discharge behaviors were investigated in stimulant cells (2016 coin-type half-cells) assembled with Ge/Ni NCAs composite as the positive electrode (cathode), a Li metal foil as the negative electrode (anode), a separator film (Celgard 2400), and a liquid electrolyte (ethylene carbonate and dimethyl carbonate (1:1 by volume)) with 1.0-M $LiPF_6$ in an Ar filled glove box. Each cell was aged for 24 h at room temperature before commencing the electrochemical tests. The galvanostatic charge-discharge measurements were conducted in a battery test system (NEWARE BTS-610, Newware Technology Co., Ltd., China) at room temperature. The cut-off voltage for the 0.1 C rate tests was 0.01–2.0 V.

Results and discussion

Fig. 1 shows a typical scanning electron microscopy (SEM) image of the NCAs. As shown in Fig. 1, most of the nanocones grew vertically to the Ni foil substrates. The average height of the cones and the mean diameter of their roots are approximately 500 nm and 180 nm, respectively. The tips of the cones are very sharp, corresponding to an apex angle of ~29°. The cone surface is rough, which is beneficial for achieving good adhesion between the deposited Ge and the current collector.

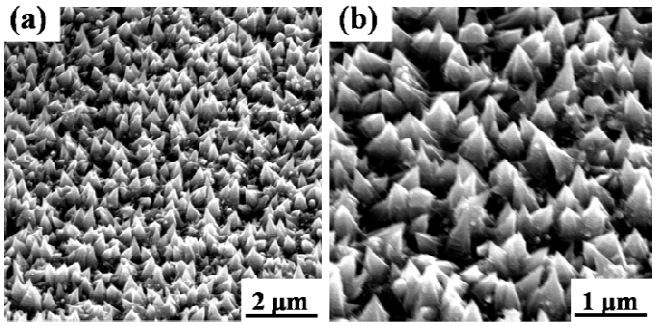

Fig. 1. SEM image (a) and its enlarged images (b) of of electrodeposited NCAs

In order to deposit germanium on the NCAs, we investigated the wettability of the ionic liquid on the NCAs. The static contact angles were measured to evaluate the wettability of the employed ionic liquid on NCAs and on the Ni foil substrate for comparison. As shown in Fig. 2, the contact angle of [Emim]Tf_2N on the Ni foil and NCAs is 47.36° and 9.03°, respectively. The contact angle considerably decreases after NCA deposition, which can be attributed to the improved roughness of the micro-nano hierarchical structure. The higher wettability of EmimTf_2N onto NCAs leads to improved penetration of the ionic liquids into the Ni nanocone cavities.

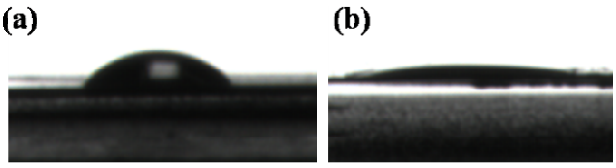

Fig. 2. Photographs of [Emim]Tf_2N droplet on surfaces (a) Ni foils and (b) NCAs.

Fig. 3 shows the cyclic voltammogram of 0.1 mol/L $GeCl_4$ in ionic liquid EmimTf_2N on the surface of NCAs. The curve reveals the two primary reduction peaks of Ge at potentials of about -0.96 and-1.47 V (compared to the Ag quasi-reference electrode), which correspond to the reduction of Ge(IV) to Ge(II) and to the reduction of Ge(II) to Ge(0), respectively.

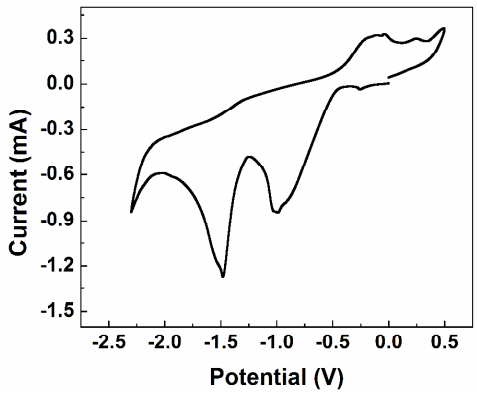

Fig. 3. Cyclic voltammogram for the electrodeposition of Ge from [Emim]Tf_2N on NCAs. The scan rate was 10 mV/s, and the test was conducted at room temperature.

Fig. 4a shows a top view of an SEM image of the Ge-NCA composite, which reveals a highly uniform coating of Ge on the surface of NCAs. After depositing the Ge, the Ni nanostructures were entirely covered with Ge cylinders with an average diameter of 800 nm. Moreover, it is evident from the SEM images that there are enough spaces between the Ge-NCAs in the resulting electrodes, which offer an opportunity for alleviating the volume expansion of Ge. The cross-sectional image of the Ge-NCA electrode on Ni foil substrate shows that the thickness of the Ge-NCAs is about 3 μm (Fig. 4b). The reduced thickness is advantageous for improving the volumetric energy density of the devices. Moreover, the Ge-NCAs thin film can be easily removed from the Ni substrate, and a freestanding Ge-NCA electrode is obtained. The image of the Ge-NCA electrode is shown in ESI,† Fig.S1b.

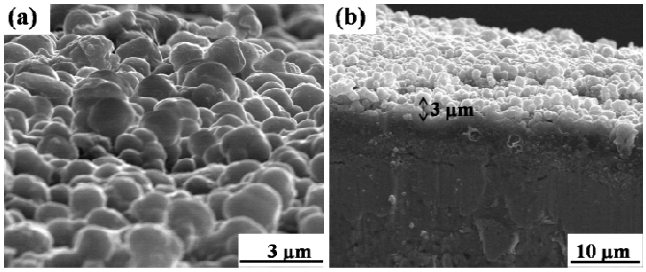

Fig. 4. (a) The SEM image of a Ge-NCA electrode on Ni foil substrate and (b) the cross-section of a Ge-NCA electrode on Ni foil substrate.

After the deposition of the Ge-NCA composite, the resulting samples were directly assembled into half-cells without using any binding or conductive additives. The electrodes had a mass load of 0.39 mg of active material per cm^2, The specific capacity calculated is based on the mass of pure Ge. A 1 C rate has been defined as the theoretical capacity of Ge (1600mAh/g). Fig. 5(a) depicts the reversible capacity plotted with respect to the cycle number at a discharge/charge rate of 0.1 C, providing direct evidence of the good lithium storage performance due to the introduction of NCA substrate into the Ge-based electrode. The Ge-NCA composite electrode shows a high discharge and charge specific capacity of nearly 1171 mAh/g and 669 mAh/g in the first cycle, respectively. The irreversible capacity loss, which is rather modest (~28%), can be attributed to the solid-electrolyte interphase (SEI) formation[29]. However, the Coulombic efficiency of the Ge-NCA electrode at the second cycle is greater than 97% and the irreversible capacity loss is about 10% from the 50 cycles to 100 cycles because the NCA-supported Ge cylinders provide fast charge transfers as well as rapid electrochemical reactions. For the as-deposited Ge electrode, the capacity for the 50th cycle is 613 mAh/g. On the other hand, after 100 charge-discharge cycles, the specific capacity of the Ge-NCA composite electrode remained at 500 mAh/g, which is much higher than the Ge film electrode on Ni foil (177 mAh/g after 100 cycles). The retention rate of the Ge-NCA composite electrode is 85.9% between the 50 cycles and 100 cycles, while the retention rate of Ge on Ni foil is a mere 30.2%. After 100 cycles (ESI,† Fig. S2), the average diameter of Ge cylinders covered on the Ni nanocone arrays of the Ge-NCA electrode increases apparently, indicating a volume expansion during cycling. However, there is no evident crack formation due to the available surrounding free space offered by NCA structure. The results indicated that the cycling performance of the Ge-NCA composite electrode has been greatly improved compared to Ge on Ni foil. Considering that the Ge deposits are interlaced with the NCAs, the enhanced binding strength between the active materials and current collector is a result of the mechanical interlocking effect.

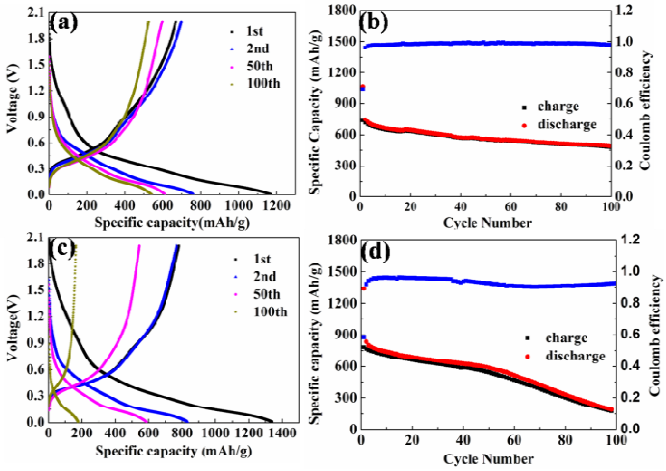

Fig. 5. (a) The charge and discharge curves and (b) the cycling performance and the Coulombic efficiency of the Ge-NCA electrode. (c) The charge and discharge curves and (d) the cycling performance and the Coulombic efficiency of the Ge-Ni foil electrode.

To investigate the rate performance of the half-cells, the lithium insertion and extraction capacities were measured at 0.1 C, 0.2 C, 0.5 C, 1 C, 2 C, and 5 C (Fig. 6). A high capacity of over 900 mAh/g is demonstrated at 0.1 C and 0.2 C. After the first 20 cycles, the discharge-charge rate was increased to 0.5 C, the capacity maintained a steady value of about 800 mAh/g. When the rate was increased to 1.0 C, a small decrease in the discharge capacity from 800 to 700 mAh/g was observed for the Ge-NCAs electrode. At higher rates, the capacities decrease to 400 and 200 mAh/g at 2 C and 5 C, respectively. However, when the rate returns to 0.1 C, the discharge capacity returns to 700 mAh/g, indicating an improved stability of the Ge-NCAs composite electrode.

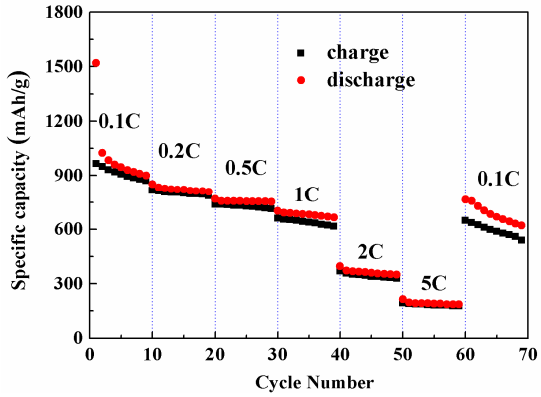

Fig. 6. Rate performance of Ge-NCAs electrode at 0.1 C, 0.2 C, 0.5 C, 1 C, 2 C, and 5 C.

The ionic conductivity of the electrolyte in the Ge-NCA electrode was confirmed by electrochemical impedance spectroscopy (EIS). Fig.7 shows the comparison of the Nyquist plots for the Ge-Ni foil and Ge-NCA electrode. Apparently, the Ge-NCA electrode shows a much lower charge-transfer resistance (Rct), than that of the Ge electrode (75 vs. 220Ω). After 100 cycles, the charge-transfer resistance of the Ge-NCA and Ge-Ni foil electrode increase to 150 and 460 Ω, respectively in the Nyquist plots. The result indicates that the Ge-NCA electrode possesses a higher electrical conductivity, which results in a better rate capability and higher reversible capacity in comparison with the Ge-Ni foil electrode.

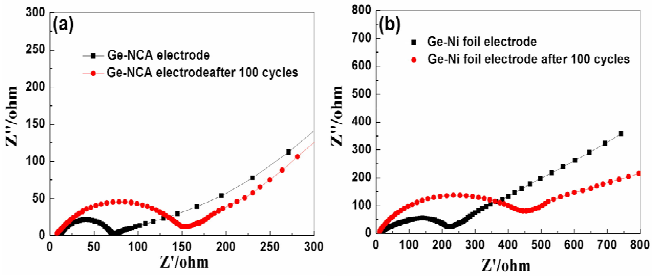

Fig. 7 Impedance spectra for Ge-NCA electrode (a) and Ge- Ni foil electrode (b). (The black line is before cycling and the red line is after 100 cycles).

The improved electrochemistry performance of the Ge-NCA electrode compared to that of block Ge is due to the interaction of the unique microstructure. First, the nanosized particles provide a higher surface area and shorter pathways for the lithium reactions. Second, the germanium films electrodeposited from ionic liquids are made of nanocrystalline and amorphous Ge[30, 31]. The presence of the nanocrystalline and amorphous phases may shorten the lithium diffusion path, and improve the electrochemical performance. The crystalline to amorphous/crystalline phase transformation is beneficial for improving not only the cycling stability but also the rate capability[32]. Third, the higher adhesion between the Ge nanoparticles and NCAs, the enhancement of the electrode surface, the good porosity of the Ge-NCAs nanostructure, which provides an available transport channel and reduces the diffusion path, and the structure of the vertical Ni nanocones increased the efficiency of electrolyte diffusion, which leads to a rate performance enhancement. In addition, the well-aligned NCAs enlarged the contact area between the Ge nanostructure and NCAs. This unique nanostructure acted as a confining buffer to accommodate enormous volume variations and relieve the large associated stresses owing to repeated Li alloying/dealloying with Ge, which keeps the germanium and lithium in close proximity after the discharge cycles. Therefore, the unique nanostructure enhances the kinetics of the lithium germanium alloy. The presence of NCAs in the nanostructure clearly plays an important role in improving the electrode energy density, which further improves the entire electrochemical performance of the electrode. Overall, the capability of delivering high capacity makes Ge-NCAs one of the most favorable candidates for a high performance anode for LIBs.

Conclusions

In summary, we report the deposition of Ge onto highly ordered freestanding NCAs from ionic liquids at room temperature for LIB electrodes. Compared with the Ge-Ni foil electrode, this unique nanostructure electrode shows a cycling capability of over 500 mAh/g after 100 cycles. The improved cycling performance of this structure is attributed to NCAs. These NCAs functioned as structural support, electron transport paths, and the inactive confining buffer. Compared with conventional methods, this fabrication method represents a viable and green approach for the direct assembly of freestanding electrodes without a binder. Improved mechanical performance and electrochemical stability of the electrode were demonstrated. Moreover, such materials present a viable alternative to conventional graphite electrodes in LIBs. Given the outstanding performance characteristics, these 3D nano-electrodes may be

suitable for high-power applications such as electric vehicles and power tools.

Acknowledgements

We thank National Natural Science Foundation of China (no. 51010005, 91216123, 51174063), Natural Science Funds for Distinguished Young Scholar of Heilongjiang province, The Natural Science Foundation of Heilongjiang Province (E201436), the International Science & Technology Cooperation Program of China (2013DFR10630) and Specialized Research Fund for the Doctoral Program of Higher Education (SRFDP 20132302110031).

Notes and references

[a] School of Chemical Engineering and Technology , Harbin Institute of Technology, 150001, Harbin, China Fax: 086 45186402345; Tel: 086 451 86403767; E-mail: jiupengzhao@126.com.
[b] State Key Laboratory of Advanced Welding and Joining, Harbin Institute of Technology, Harbin 150001, China.
[c] Center for Composite Material, Harbin Institute of Technology, Harbin 150001, China, liyao@hit.edu.cn.
[d] Shanghai Institute of Applied Physics, Chinese Academy of Sciences Shanghai 201800, China.

Electronic Supplementary Information (ESI) available: [The photos of Ge-NCA/Ni films and the freestanding Ge-NCA and SEM image of Ge-NCA electrode after 100 cycles at 0.1 C]. See DOI: 10.1039/b000000x/

‡ These two authors contributed equally to this work.

1. M. Beidaghi and Y. Gogotsi, *Energ Environ Sci*, 2014, **7**, 867-884.
2. B. Dunn, H. Kamath and J. M. Tarascon, *Science*, 2011, **334**, 928-935.
3. I. Kovalenko, B. Zdyrko, A. Magasinski, B. Hertzberg, Z. Milicev, R. Burtovyy, I. Luzinov and G. Yushin, *Science*, 2011, **334**, 75-79.
4. K. Evanoff, A. Magasinski, J. B. Yang and G. Yushin, *Adv Energy Mater*, 2011, **1**, 495-498.
5. Y. J. Cho, H. S. Im, H. S. Kim, Y. Myung, S. H. Back, Y. R. Lim, C. S. Jung, D. M. Jang, J. Park, E. H. Cha, W. Il Cho, F. Shojaei and H. S. Kang, *Acs Nano*, 2013, **7**, 9075-9084.
6. M. H. Park, Y. Cho, K. Kim, J. Kim, M. L. Liu and J. Cho, *Angew Chem Int Edit*, 2011, **50**, 9647-9650.
7. M. H. Park, K. Kim, J. Kim and J. Cho, *Adv Mater*, 2010, **22**, 415-+.
8. X. L. Wu, Y. G. Guo and L. J. Wan, *Chem-Asian J*, 2013, **8**, 1948-1958.
9. W. Li, J. Zheng, T. K. Chen, T. Wang, X. J. Wang and X. G. Li, *Chem Commun*, 2014, **50**, 2052-2054.
10. G. H. Yue, X. Q. Zhang, Y. C. Zhao, Q. S. Xie, X. X. Zhang and D. L. Peng, *Rsc Adv*, 2014, **4**, 21450-21455.
11. J. Li, C. Yue, Y. J. Yu, Y. S. Chui, J. Yin, Z. G. Wu, C. D. Wang, Y. S. Zang, W. Lin, J. T. Li, S. T. Wu and Q. H. Wu, *J Mater Chem A*, 2013, **1**, 14344-14349.
12. I. S. Hwang, J. C. Kim, S. D. Seo, S. Lee, J. H. Lee and D. W. Kim, *Chem Commun*, 2012, **48**, 7061-7063.
13. S. F. Fan, L. Y. Lim, Y. Y. Tay, S. S. Pramana, X. H. Rui, M. K. Samani, Q. Y. Yan, B. K. Tay, M. F. Toney and H. H. Hng, *J Mater Chem A*, 2013, **1**, 14577-14585.
14. D. J. Xue, S. Xin, Y. Yan, K. C. Jiang, Y. X. Yin, Y. G. Guo and L. J. Wan, *J Am Chem Soc*, 2012, **134**, 2512-2515.
15. Z. M. Cui, L. Y. Hang, W. G. Song and Y. G. Guo, *Chem Mater*, 2009, **21**, 1162-1166.
16. D. K. Kim, P. Muralidharan, H. W. Lee, R. Ruffo, Y. Yang, C. K. Chan, H. Peng, R. A. Huggins and Y. Cui, *Nano Lett*, 2008, **8**, 3948-3952.
17. X. L. Xiao, L. M. Yang, H. Zhao, Z. B. Hu and Y. D. Li, *Nano Res*, 2012, **5**, 27-32.
18. X. L. Wu, Q. Liu, Y. G. Guo and W. G. Song, *Electrochem Commun*, 2009, **11**, 1468-1471.
19. M. H. Park, M. G. Kim, J. Joo, K. Kim, J. Kim, S. Ahn, Y. Cui and J. Cho, *Nano Lett*, 2009, **9**, 3844-3847.
20. H. Kim, B. Han, J. Choo and J. Cho, *Angew Chem Int Edit*, 2008, **47**, 10151-10154.
21. T. Song, J. L. Xia, J. H. Lee, D. H. Lee, M. S. Kwon, J. M. Choi, J. Wu, S. K. Doo, H. Chang, W. Il Park, D. S. Zang, H. Kim, Y. G. Huang, K. C. Hwang, J. A. Rogers and U. Paik, *Nano Lett*, 2010, **10**, 1710-1716.
22. S. H. Tang, E. Y. Chang, M. Hudait, J. S. Maa, C. W. Liu, G. L. Luo, H. D. Trinh and Y. H. Su, *Appl Phys Lett*, 2011, **98**.
23. N. G. Rudawski, B. L. Darby, B. R. Yates, K. S. Jones, R. G. Elliman and A. A. Volinsky, *Appl Phys Lett*, 2012, **100**.
24. B. Laforge, L. Levan-Jodin, R. Salot and A. Billard, *J Electrochem Soc*, 2008, **155**, A181-A188.
25. F. Endres and S. Z. El Abedin, *Phys Chem Chem Phys*, 2006, **8**, 2101-2116.
26. J. Graetz, C. C. Ahn, R. Yazami and B. Fultz, *J Electrochem Soc*, 2004, **151**, A698-A702.
27. Z. J. Du and S. C. Zhang, *J Phys Chem C*, 2011, **115**, 23603-23609.
28. D. S. Wang, Z. B. Yang, F. Li, X. H. Wang, D. Q. Liu, P. Wang and D. Y. He, *Mater Lett*, 2011, **65**, 3227-3229.
29. A. Magasinski, P. Dixon, B. Hertzberg, A. Kvit, J. Ayala and G. Yushin, *Nat Mater*, 2010, **9**, 461-461.
30. X. Liu, J. P. Zhao, J. Hao, B. L. Su and Y. Li, *J Mater Chem A*, 2013, **1**, 15076-15081.
31. J. Hao, X. X. Liu, N. Li, X. S. Liu, X. X. Ma, Y. Zhang, Y. Li and J. P. Zhao, *Rsc Adv*, 2014, **4**, 60371-60375.
32. L. Y. Lim, N. Liu, Y. Cui and M. F. Toney, *Chem Mater*, 2014, **26**, 3739-3746.